

# HiSST: 4th International Conference on High-Speed Vehicle Science Technology



22 -26 September 2025, Tours, France

# Current Status and Applications of CoNF<sup>2</sup>aS<sup>2</sup> – Coupled Numerical Fluid Flight Mechanics and Structure Simulation

V. Wartemann<sup>1</sup>, M. Franze, S. Jack, F. Barz, B. Reimann

#### Abstract

The Coupled Numerical Fluid Flight Mechanics and Structure Simulation (CoNF<sup>2</sup>aS<sup>2</sup>) tool is a DLRdeveloped coupling environment specifically designed for spacecraft applications. As the name already implies, the focus of CoNF<sup>2</sup>aS<sup>2</sup> lies in the interactions between fluid, thermal, structural and flight mechanics for aerodynamic and aerothermal load calculations. Like any numerical tool, the continuous upgrade of CoNF<sup>2</sup>aS<sup>2</sup> through wind tunnel experiments and flight tests is an ongoing process with a permanent expansion of its application possibilities. The main goal of CoNF<sup>2</sup>aS<sup>2</sup> is to achieve realistic simulations of space transportation vehicles in their entire flight range. This paper presents validation examples as well as an overview of the current development status of CoNF<sup>2</sup>aS<sup>2</sup>. Some of the possible fidelity levels of  $CoNF^2aS^2$  are introduced and accompanied by example applications.

Keywords: CoNF<sup>2</sup>aS<sup>2</sup>, Coupled CFD Simulation, Aerothermal Loads, Deformation, SHEFEX II, ReFEX, Rocket Nozzle, Panel Flutter, High-Lift Reentry Vehicles

#### Nomenclature

Abbreviations		MORABA	Mobile Rocket Base of the DLR
ARFL CFD CoNF <sup>2</sup> aS <sup>2</sup> CPU CSM	US Air Force Research Laboratory Computational Fluid Dynamics Coupled Numerical Fluid Flight Me- chanic and Structure Simulation Central Processing Unit Computational Structural Mechanics	MPI PSD ReFEx SHEFEX RLV TPS	Message Passing Interface Power Spectral Density Reusability Flight Experiment SHarp Edge Flight EXperiment Reusable Launch Vehicle Thermal Protection System
DLR	German Aerospace Center	Latin	
EoE	End of Experiment	h	Altitude
FS	FlowSimulator	M	Mach number
FSDM	FlowSimulator Data Manager	p	Pressure
FSI	Fluid-Structure Interaction	T	Temperature
HGV	Hypersonic Glide Vehicles	t	Time
HPC	High-Performance Computing	Greek	
KTR	Koonibba Test Range	$\alpha$	Angle of attack

#### 1. Introduction

Aerothermodynamics has historically presented some of the most significant challenges in the realm of hypersonic flight. The high temperatures generated by shock waves and friction at hypersonic speeds result in a variety of physical phenomena, which are still challenging for the successful design of viable, longduration hypersonic vehicles. Recent literature reviews and studies by Russel [8] have identified several key challenges associated with hypersonic flight. A challenge-list summarized by Morgan [29] includes following topics: High heating rates, viscous forces and drag, high temperature plasmas generated stability and control issues, fluid/thermal/structural issues, materials challenges, radiation signatures, sonic

<sup>&</sup>lt;sup>1</sup>German Aerospace Center (DLR), Spacecraft Department, Institute of Aerodynamics and Flow Technology, Braunschweig, Germany, Viola. Wartemann@dlr.de, Marius.Franze@dlr.de, Sebastian. Jack@dlr. de, Fynn. Barz@dlr. de, Bodo. Reimann@dlr. de

booms, ablation, complicated chemical interaction with flow field, challenging propulsion systems, challenging vehicle design issues (inlets, nozzles, waverider, etc.). To address these various effects and their combinations, the DLR coupling environment  $\text{CoNF}^2\text{aS}^2$  was developed. The main goal of  $\text{CoNF}^2\text{aS}^2$  is to achieve realistic simulations of space transportation vehicles across their entire flight range, including the critical hypersonic regime. This paper focuses on a subset of these challenges: fluid/thermal/structural interactions and vehicle designs, demonstrating how the DLR  $\text{CoNF}^2\text{aS}^2$  tool chain can be applied to address them.

### 2. Introduction of CoNF<sup>2</sup>aS<sup>2</sup>

To provide realistic simulations, the question typically arises about the flight range: is the whole trajectory of interest or just parts of it? Is a specific flight range of interest? Can other parts be neglected? As mentioned above, the more complex hypersonic flight range has a longer list of issues than other flight ranges. Furthermore, many effects depend on the geometry itself and its complexity. Additionally, the combinations of different effects play a role. Therefore, to reproduce reality, coupled simulations are recommended.

The knowledge of the necessary combination of disciplines dates back a long time. The initial coupling ideas and approaches of the Department of Spacecraft in Braunschweig were around 2000, see e.g. [25]. Important validation steps for the coupling environment were the SHEFEX I post-flight analysis, as described in Barth et al. [2, 3]. The SHarp Edge Flight Experiments (SHEFEX) of the DLR have been established to demonstrate the feasibility of space vehicles with facetted Thermal Protection Systems (TPS) by keeping or improving aerodynamic properties. The TPS consists of simple flat panels with sharp edges and without any constraints on system compatibility and reliability of space vehicles. SHE-FEX I was started from northern Norway's Andøya Rocket Range in October 2005 and can be seen as the first validation case of the multi-fidelity coupling, although based on coupled approaches of a predecessor of CoNF<sup>2</sup>aS<sup>2</sup>. The official CoNF<sup>2</sup>aS<sup>2</sup> label for a numerical post-flight analysis can be applied to the SHEFEX II flight (see section 3: Validation of CoNF<sup>2</sup>aS<sup>2</sup>). CoNF<sup>2</sup>aS<sup>2</sup> as coupling environment of the DLR Spacecraft Department in Braunschweig, builds on top of the so-called DLR FlowSimulator (FS). This is a software integration framework for HPC(high-performance computing)-ready multidisciplinary simulations, jointly developed by AIRBUS, DLR, and ONERA. CoNF<sup>2</sup>aS<sup>2</sup> builds on top of the FlowSimulator, heavily utilizing its functionality and adding more within its own framework, necessary for spacecraft applications.

The FlowSimulator itself is organized in three layers (see figure 1) [32]: At the top is the control layer, which is the end user's main access layer, based on python scripts. The FSDataManager (FSDM) is the data layer, which enables in-memory data exchange and is designed for full parallelism, supporting existing intra-solver and (optional) inter-solver parallelism via Message Passing Interface (MPI). The plugin layer comprises the set of all applications/tools interfacing with the FSDM and being available for use in FlowSimulator. For detailed information on the FlowSimulator, consult e.g. [31, 32]. The main advantage of this coupling environment is the in-memory data exchange, which prevents the most time-consuming part: reading input and writing output, short file I/O. This approach saves unnecessary extra time and disc space, by writing only results and no additional intermediate files.

The focus of this paper is on the DLR CoNF<sup>2</sup>aS<sup>2</sup> tool chain, the add-on coupling environment for space-craft applications, including additional spacecraft related tools, see figure 2. The focus here in this paper is on the Fluid–Structure Interaction (FSI), the coupling of a CFD solver with a CSM solver to consider the heating as well as the deformation process. Different fidelity approaches in CoNF<sup>2</sup>aS<sup>2</sup> are applicable. Depending mainly on the test case and the scientific question, the accuracy of the solver can be chosen. Especially high-fidelity FSI coupled simulations along whole trajectories can be intensive in terms of time, total CPU hours and data sizes. Less accurate methods are cheaper but cannot cover the same quality of results. Thus a practical guiding principle is: High-fidelity if necessary and low-fidelity if possible. The highest accuracy is naturally attended by the highest numerical effort. For example, as high-fidelity fluid solver, the DLR TAU code, also in diverse accuracy levels can be chosen (e.g. RANS

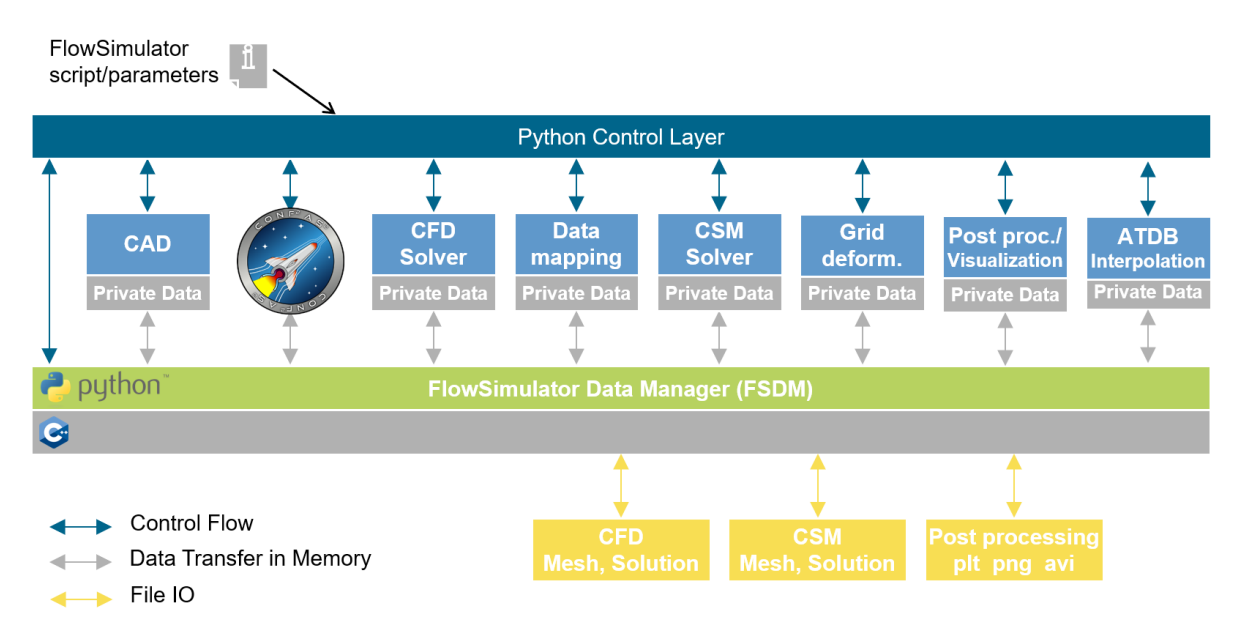


Fig 1. Schema of the DLR FlowSimulator framework.

including chemical reactions), here marked as FSTAU (RANS) plug-in. As high-fidelity structure solver currently only the commercial Ansys solver (plug-in name: FSAnsysInterface) is available. Examples of high-fidelity applications can be found in chapter 3 and 6. The mid-fidelity approach is explained in detail in chapter 4 and is visualised in figure 2 as FSTAU (Euler) in combinations with FSHeatFluxInterpolation. Especially for the layout processes faster simulations methods are required. The low-fidelity plug-ins are summarized in figure 2 as FSPanelCFD and FSStructureHeating and are described with an example application in chapter 5.

If necessary, additional tools and models can be added to the CoNF<sup>2</sup>aS<sup>2</sup> tool chain like Atmosphere models, gravitational models, flight mechanics or flight controllers. If an investigation along a trajectory is performed, it is possible to switch between accuracy levels as well as to add additional models or tools along the trajectory. For example, depending on the altitude a switch of the CFD approach is necessary (e.g. from laminar to turbulent) or it is possible to reduced the accuracy along the trajectory due to the change of the flight regime and/or not all parts of the trajectory are from special interest or has not an high influence, depending on the scientific question. A good literature status summary of coupling analyses performed by other research facilities and institutions, sorted by the accuracy levels is given by Franze et al. [12].

### 3. Validation of CoNF<sup>2</sup>aS<sup>2</sup> applying coupled high-fidelity simulations

Two validation examples are given in this section, which are focused on FSI. The most prominent CoNF<sup>2</sup>aS<sup>2</sup> validation test case is summarized in subsection 3.1 based on the post-flight analysis of the SHEFEX II flight. The second validation example is focused on one part of a space transportation vehicle, the rocket nozzle and the effect of deformation.

For both high-fidelity analyses the FSI is performed fully strong coupled with a CFD solver in partitioned scheme with a CSM solver. The load transfer is achieved through marker-based interpolations from the CFD interface mesh to the CSM interface mesh and vice versa. As CFD solver the DLR TAU code is applied, which is a three-dimensional parallel hybrid multigrid solver that has been validated for subsonic, transonic, and hypersonic flows (as demonstrated in, e.g., Langer et al. [22], Mack et al. [26] or Schwamborn et al. [34]). It solves the Reynolds-Averaged Navier-Stokes (RANS) equations using a second-order finite-volume method and is optimized for large-scale simulations on HPC systems. For the

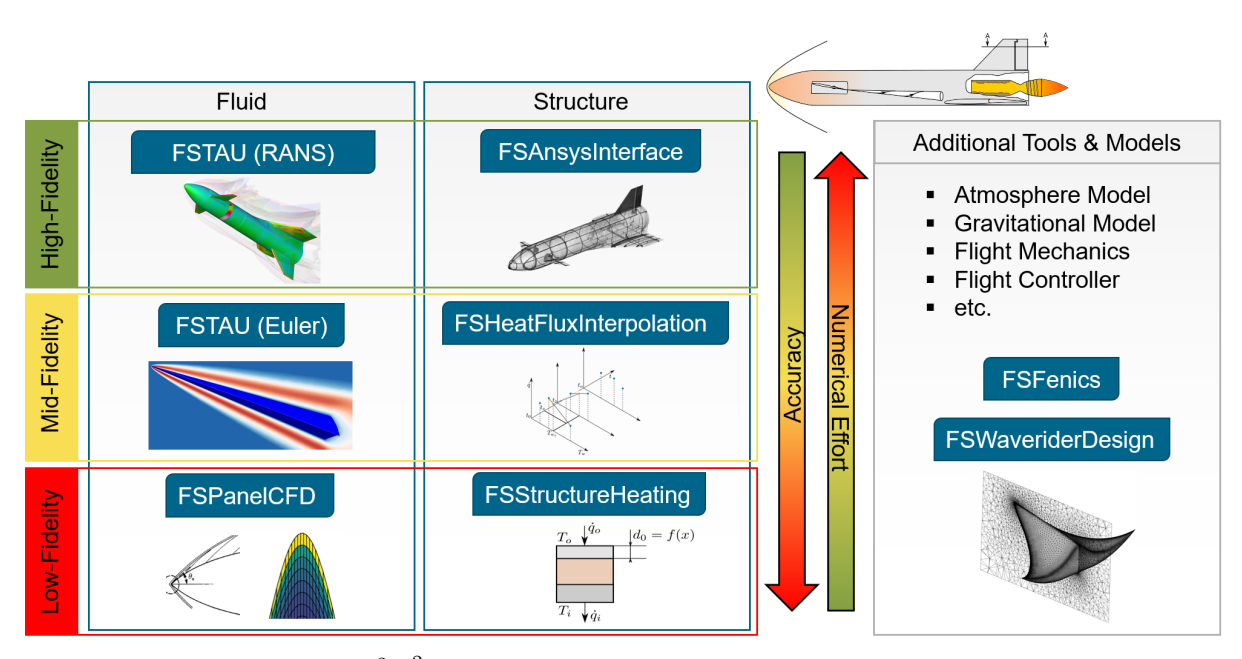


Fig 2. DLR CoNF<sup>2</sup>aS<sup>2</sup> and FlowSimulator Plug-ins, DLR (CC BY-NC-ND 4.0).

CSM sover the commercial Ansys Mechanical code is used.

#### 3.1. SHEFEX II

In June 2012 the SHEFEX II flight took place from Andoya Rocket Range, Norway. The main objective of the second SHEFEX flight was to successfully conduct a hypersonic re-entry with a fully aerodynamically controlled vehicle. During the flight, the speed range was extended to a maximum Mach number of 11, compared to SHEFEX I. Apart from the extension of the flight regime the vehicle contains four independently controllable canards for the active control of the re-entry flight. These sharp edged ceramic canards and the facetted ceramic TPS were the key experiments of SHEFEX II, see e.g. Weihs et al. [35].

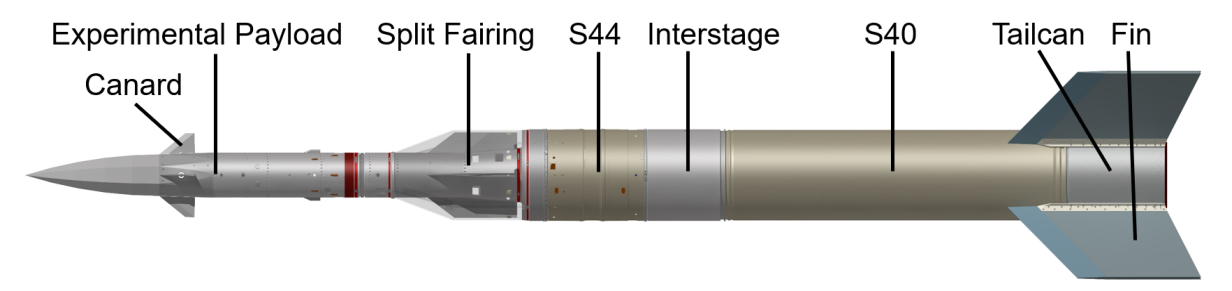


Fig 3. Schematic representation of SHEFEX II, reprinted from [14].

Figure 3 shows the launch configuration of SHEFEX II with a total length of  $12.76\,\mathrm{m}$ . It consists of two stages: The first stage is a Brazilian S40 motor and the second stage a Brazilian S44 motor. More than 140 sensors, including surface pressure and temperature sensors, investigated the overall behavior of the ceramic tiles and surrounding flow conditions as well as the controlling flight performance of the canards. The data is utilized for the validation of  $\mathrm{CoNF^2aS^2}$ . This extensive validation is based on the ascent phase of the launch, the first  $60\,\mathrm{s}$  of the flight up to a mach number of 4.8. The post-flight analysis revealed that the following two factors are crucial for matching reality:

- Reconstructed wind profiles, as demonstrated by Franze et al. [14]
- Structural deformation, as shown by Franze [12]

Including these beside the thrust profile based on ground experiments, the simulation results are very close to the reality, e.g. the measured angle of attack. The deviations of the oscillation curve of the aerodynamic angle of attack are  $-0.23^{\circ}$  to  $0.44^{\circ}$  during the first 30 s of the launch phase and less than  $\pm 0.9^{\circ}$  after the engine burnout.[12] The key findings of the post-flight analysis of SHEFEX II using thermal and mechanical coupled fluid-structure simulations is:

• The uncertainty of the numerical results is less than in the flight experiments, if structural deformation and wind model is considered.

The only limitation is given by the capabilities of the applied codes itself. Consequently, the CoNF<sup>2</sup>aS<sup>2</sup> validation is demonstrated for the here shown flight range and its resulting flow phenomena. A movie of the coupled CoNF<sup>2</sup>aS<sup>2</sup> simulation can be seen via QR-code of figure 4(a). For more details following papers are recommended: Franze et al. [9, 10, 11, 12, 14].

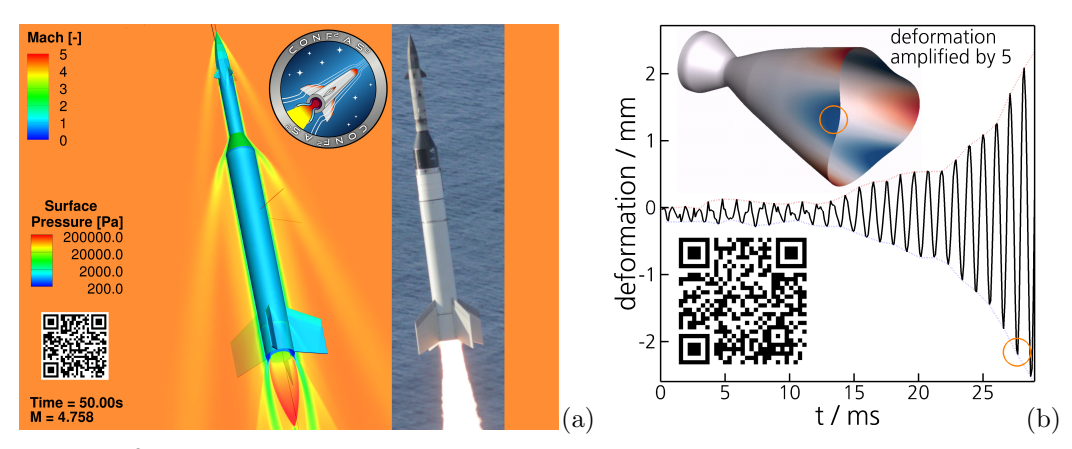


**Fig 4.** CoNF<sup>2</sup>aS<sup>2</sup> validation test cases: Post-flight analysis of the DLR SHEFEX-II flight (a) and flexible rocket nozzle (b), DLR (CC BY-NC-ND 4.0).

### 3.2. Flexible sub-scale rocket nozzle

The dynamic deformation of the thrust nozzle represents a complex overall system due to the mutual interaction of the complex phenomena in the detached inner supersonic flow and the deformation of the lightweight structure, which is in the focus of this validation subsection. In the context of the DLR project AMADEUS, an experiment was designed and built to investigate fluid-structure interaction in highly overexpanded separated nozzle flows. Based on the preceeding systematic analysis of isolated effects [17, 16, 18, 19] the CoNF<sup>2</sup>aS<sup>2</sup> tool chain firstly allowed the preliminary design of a possible experimental setup to yield valuable validation data missing for this complex use case. The mechanical properties and possible experimental setups for a defined initial deformation actuation were proposed, discussed, and tested numerically in high-fidelity, ensuring sufficient strain margins for safe operation on the testbench [20]. Based on this preliminary design study, a test specimen with a stiff thrust chamber and a flexible nozzle extension with a wall thickness of 1.5 mm was produced from polycarbonate, designed for investigation in the experimental cold flow test campaign. An appropriate mechanism for initial deformation of the model as well as software to detect basic shape and frequency from high-speed images recorded during the experiments were developed. Preliminary experiments using the test specimen validated that CoNF<sup>2</sup>aS<sup>2</sup> is able to very accurately predict the structure's stiffness and eigenmodes shapes and frequencies. The experiments shows that the self-excited oscillations observed in the coupled experiment are in very good agreement with the numerical design regarding eigen-frequencies, damping characteristics and the pressure ratios at which they are observed. Figure 4(b) illustrate the simulation of a flexible nozzle for an instable setup. A movie of the coupled CoNF<sup>2</sup>aS<sup>2</sup> simulation can be seen via

QR-code of figure 4(b). The CoNF<sup>2</sup>aS<sup>2</sup> simulations are proven to be well capable to design and analyze this complex application of fluid-structure interaction.

### 4. Mid-fidelity example of CoNF<sup>2</sup>aS<sup>2</sup>

To explain the mid-fidelity approach, a Hypersonic Glide Vehicles (HGV) is selected as geometry, which is depicted in Figure 5(a). The reference length measures 3.0 m, while the width is 1.2 m, with the rounded leading edge excluded from consideration. The radius of the leading edge is 4.5 mm. To streamline the calculations, the body flaps illustrated in the figure were not modeled in this subsection's simulations, as the primary focus was on heating process of the main body. The body itself was designed using an osculating cone method at a design Mach number of 10 with a semi-vertical angle of the conical shock between the rotational axis and the shock itself of 10°, shaping the base edge. Consult for more details Barz et al. [4].

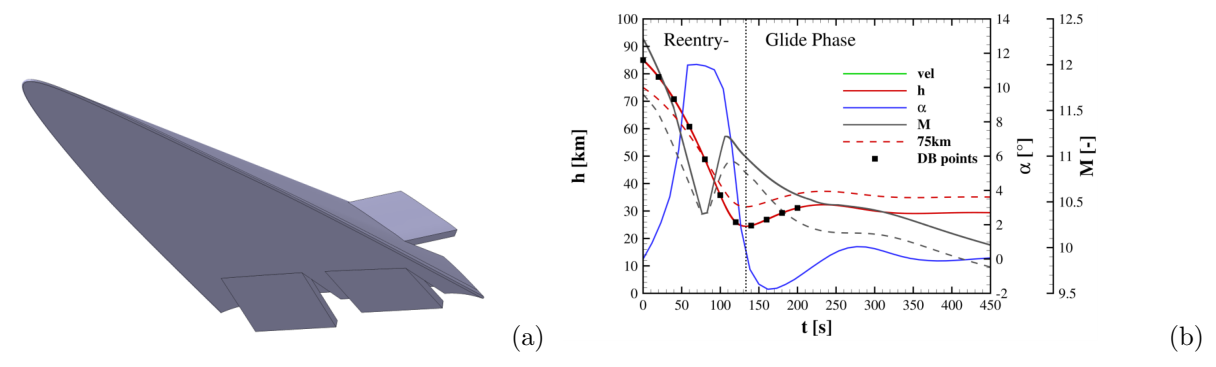


**Fig 5.** Schematic of the HGV Geometry (a) and generic trajectory including altitude, angle of attack and Mach number for starting altitude at 85 km and 75 km with marked points for database generation (b), reprinted from [13].

Figure 5(b) presents the generic trajectories, showing the altitude h, angle of attack  $\alpha$  and Mach number M over the time. The initial trajectory (lines) starts at t=0 s with a motor separation at an altitude of 85 km. This maneuver is followed by a dipping reentry curve. Following by the cruise phase, which begins at t=200 s.

Usually depending on the reentry mission profile, the TPS is a crucial point in design for these configurations. It needs to withstand the high heat fluxes while being robust and light-weight. As first steps the coupled high-fidelity simulation is performed with a calculated time step size of  $\Delta t = 0.1$  s. This can be time consuming and computational expensive. Depending on the flight path this can easily lead to months of computation time. Thus, once one loop of the high-fidelity methods is performed, as second step an Aero-Thermal Database (ATDB) [23] approach finds its application as mid-fidelity method as a much faster surrogate model for heating. The database consists in this case of 11 selected time points at  $\Delta t = 20$  s (marked in figure 5(b) as black points) from the unsteady high-fidelity solution by reusing their converged solutions. Then a second steady solution at each point with a higher impinged surface temperature of  $\Delta T = 200\,\mathrm{K}$  is calculated. This results in 2 data points at each given altitude to get a gradient to account for the influence of local wall temperature on the resulting heat flux. This mid-fidelity CFD solution provides the new heat flux on the surface as a bi-linear interpolated function of altitude and local surface temperature, then gets locally interpolated on the CSM mesh along the unsteady solution process within CoNF<sup>2</sup>aS<sup>2</sup>. The CSM solver is the same, used for the high-fidelity coupling scheme, lowering the computation time to some days for the whole  $t = 450 \,\mathrm{s}$  of the trajectory. The calculated time steps are  $\Delta t=1.0 s$ .

Figure 6(a) compares the CoNF<sup>2</sup>aS<sup>2</sup> mid-fidelity solution with the CoNF<sup>2</sup>aS<sup>2</sup> fully coupled high-fidelity results at 200 s. The peak difference in temperature at the nose tip is  $\Delta T < 8 \,\mathrm{K}$  at a total amount of 2387 K in the interpolated case. In the worst-case scenario at  $x = -2.0 \,\mathrm{m}$  on the symmetry cut,

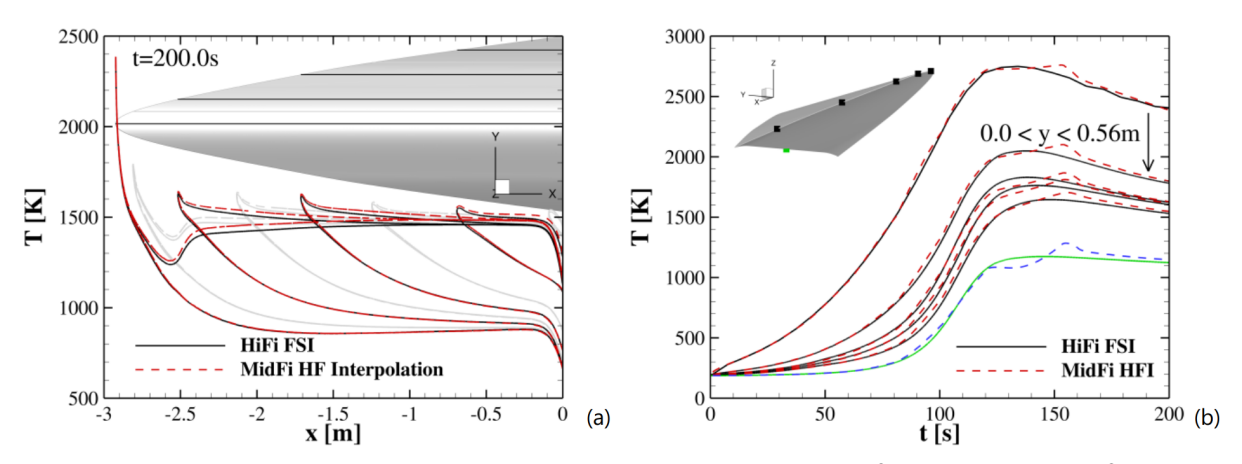


Fig 6. Differences in structural heating between fully coupled CoNF<sup>2</sup>aS<sup>2</sup> FSI and CoNF<sup>2</sup>aS<sup>2</sup> heatflux interpolation from database, reprinted from [13].

the predicted temperatures are  $\Delta T = 33 \,\mathrm{K}$  higher at  $1455 \,\mathrm{K}$  on the lee side compared to the fully coupled transient solution. Considering the significantly faster solution time of several magnitudes, these differences are negligible. The heating on the lee side of the HGV matches very well between the two coupled procedures because it is dominated by in-body heat conduction, which is calculated by the same CSM solver. During the temperature evolution shown in figure 6(b) over time, some oscillations are present between  $t = 120 \,\mathrm{s}$  and  $t = 160 \,\mathrm{s}$ , where the interpolation databases lack the transition from reentry to glide phase. The biggest difference is  $\Delta T = 108\,\mathrm{K}$  at the leading edge at  $t = 154\,\mathrm{s}$ , which again is reasonable and can be improved by adding more data points. As the glide phase characteristics get represented in great detail, the much faster method can now be applied for example to calculate the trajectory from 0 s < t < 450 s or to calculate a complete new trajectory (see dashed line in figure 5(b), reusing the generated database, which was performed by Franze et al. in [13]).

A detailed investigation of the mid-fidelity AeroThermal Database Interpolation method integrated in CoNF<sup>2</sup>aS<sup>2</sup> and compared to high-fidelity CoNF<sup>2</sup>aS<sup>2</sup> FSI simulations is given in Franze et al. [13]. The short summary of the analysis of Franze et al. [13] in this paper demonstrates a multi-fidelity approach, which can be used to accelerate the design process. The faster CoNF<sup>2</sup>aS<sup>2</sup> mid-fidelity method enables e.g. trajectory optimizations and fast evaluations of material combinations and variations.

## 5. Low-fidelity example of $CoNF^2aS^2$

This example illustrates the application of low-fidelity solvers coupled within the  $\text{CoNF}^2\!\text{aS}^2$  environment. The mission and vehicle are identical to those described in section 4. In this scenario, the heating of the structure is calculated using the FSStructureHeating plug-in. The plug-in solves the one-dimensional transient heat conduction equation, with the direction of conduction determined by the local surface normal. Within the plug-in, the material of every element can be specified as a stack of materials with a distinct height. This feature enables the modelling of structures, such as thermal protection systems, featuring an outer ceramic layer, insulation and an inner structure. Furthermore, the boundary conditions can be set to an adiabatic wall, constant temperature or heat flux. An additional feature is the simulation of the heat radiation by the gray body model.

For the HGV example, all features are utilized. The full ceramic leading edge, nose and outer layer as well as the isolation and inner aluminum structure of the HGV are modelled with distinct thicknesses at every element. The HGV is defined as hollow shape, with the inner surface defined as adiabatic wall. On the outer surface, the heat flux is prescribed by the solution of the low-fidelity aerothermodynamic solver, FSPanelCFD, and the radiation of the gray body radiation model.

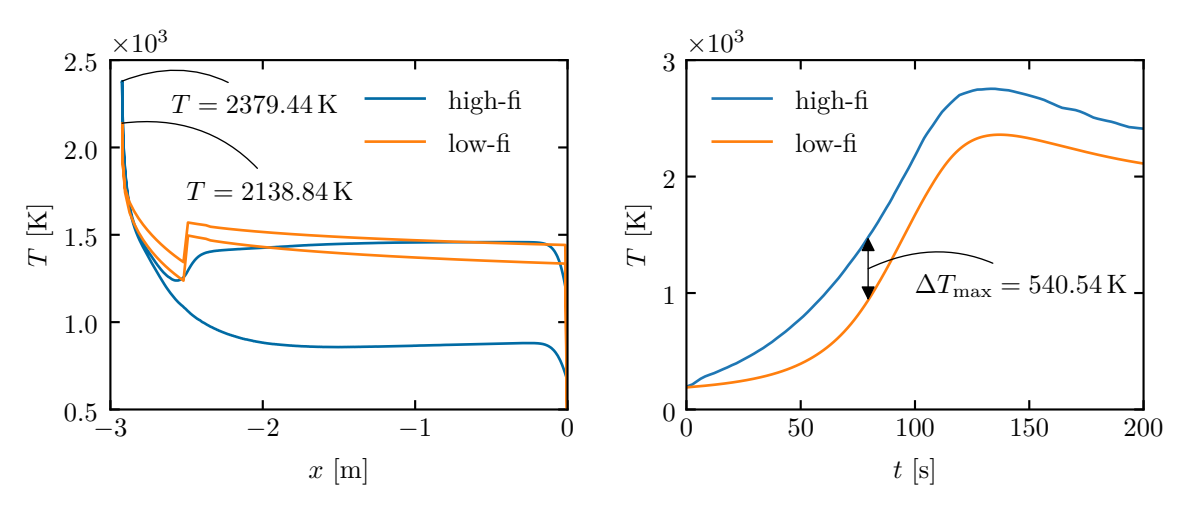
As the name implies, the flow solution is calculated by the inclination of the local surface panels. Several

methods for inviscid super- and hypersonic flows of perfect gases are available within the plug-in, including: the shock expansion method [1] for slender sharp leading edged geometries, the modified Newton method [1] for blunt bodies, a combination of both with the matching point method [21] and the piston theory [24]. The viscous contribution can be taken into account by the reference temperature method [1] and solutions of the laminar or turbulent boundary layer equation [1, 5]. The aerothermodynamic heating effects can be calculated by the Reynolds analogy for flat surfaces or the solution of the Fay-Riddell equation in conjunction with correlations for cylinders in cross flow [1].

In this example case, the aerodynamics is calculated by the matching point method. Thus, the blunt leading edge is evaluated by the modified Newton method until the point downstream where the pressure and pressure gradient match those for the shock expansion method. From this point, the surface state is evaluated by the shock expansion method. The aerothermodynamic heating in the leading edge region is calculated by combining the Fay-Riddell equation with the cylinder correlation. The reference temperature method is conducted in the region downstream the matching point.

The heating along the trajectory is performed by a loose coupling with a time step size of  $\Delta t = 0.5 \,\mathrm{s}$ . The results are presented in figure 7 which compares the low-fidelity with high-fidelity results from Franze et al. [13]. The temperature distribution in the symmetry plane is depicted in the figure 7(a) for the low- and high-fidelity solutions at  $t = 200 \,\mathrm{s}$ . The stagnation point shows higher temperatures in the high-fidelity solution, attributed to non-equilibrium chemistry effects. Specifically, dissociation behind the shock reduces the distance between the shock and surface, while recombination near the surface increases fluid temperature, thus heat flux. A kink in the temperature of the low-fidelity solution is observed where solid nose ends and the isolation material layer starts, which reduces the heat capacity. This feature is smoothed in the high-fidelity solution by the in plane heat conduction. Furthermore, the difference between the lux and lee temperature is smaller for the high-fidelity solution due to conduction from the lux to the lee in the solid nose, not captured by the low-fidelity model.

The figure 7(b) shows the same qualitative trend for both simulations. Differences appear until  $t \approx 75 \,\mathrm{s}$  where the high-fidelity solution exhibits increased temperature growth due to lower density at high altitudes and potential limitations of the perfect gas Fay-Riddell solution.



(a) Distribution of the surface temperature at the sym- (b) The evolution of the surface temperature at the metry plane at  $t=200\,\mathrm{s}$ .

Fig 7. Comparison of the low-fidelity results with high-fidelity results by Franze et al. [13].

The results indicate that the low-fidelity solution closely follows the high-fidelity computations, demonstrating a good correlation. This suggests that it is reasonable to use the low-fidelity solution for the initial design of HGV or as an underlying trend for a multi-fidelity optimization.

## 6. Applications and upgrades of $CoNF^2aS^2$

As first application example of this chapter the DLR ReFEx flight experiment is given (chapter 6.1). The second application is an example for the ongoing expansion of the CoNF<sup>2</sup>aS<sup>2</sup> applications, looking at the panel flutter phenomena (chapter 6.2).

### 6.1. ReFEx

One prominent CoNF<sup>2</sup>aS<sup>2</sup> application example is the hypersonic flight experiment ReFEx, which has been developed by the DLR since 2018 and is currently in the final integration stage. ReFEx has a mass of around 400 k, a length of 2.7 m and deployable wings with a span of 1.1 m. The key mission events and timeline can be seen in figure 8(a): ReFEx is launched on a VSB-30 sounding rocket, consisting of the S31 first stage and the S30 second stage provided by MORABA, starting from the Koonibba Test Range (KTR) in southern Australia in 2026. After separating the fairings, ReFEx actual experimental mission begins: ReFEx unfold its wings, which were stored underneath the fairing; the Mach number of ReFEx will be up to M=5 and the altitude around 135 km. The initial deceleration is performed at high angles of attack. The orientation counterintuitively in a belly-up position. Once ReFEx reaches the lower regions of the atmosphere, it performs a roll maneuver to the belly-down position. In this flight phase, the angle of attack is decreased to fly at angles close to a state of the maximum lift-to-drag ratio and continue the flight to EoE. The planned trajectory is representative of an aerodynamically controlled RLV (Reusable Launch Vehicle) booster stage, where ReFEx will test several key technologies required for future reusable aerodynamically controlled first stages.[33]

The aerodynamic design process of ReFEx consists of iteratively calculating partial datasets of different geometries, see Merrem et al. [27]. For the final geometry, a full set of aerodynamic data containing all parameter variations for all flight conditions is calculated to provide information for the flight controller to adequately command the control surfaces to adjust the vehicle's orientation. For ReFEx, the list of parameters that describes the flight condition consists of Mach number, angle of attack, sideslip angle, altitude, canard deflections (left and right), rudder deflection and rotation rates around vehicle fixed axes. The description of the dataset approach are summarized in detail by Merrem et al. [28]. In total the aerodynamic database consists of about 2400 high-fidelity (RANS) data points. One main key point during the numerical aero- and aerothermodynamic pre-analyses in the layout process of the ReFEx vehicle was the thermal analysis, which is investigated in detail by Franze et al. [15]: The usually following DLR development process applies, in general, the classical V-model of systems engineering to analyze a first design space and achieve possible solutions. Due to the complex ReFEx mission requirements a lot of variables had to be considered at the beginning (e.g. trajectories, sizing, launcher systems, etc.). To handle this early in the project (pre-phase/phase A) in an economic way, an additional agile design loop was introduced into the V-model by developing an extended dataset based thermo-mechanic analysis (in the following named: V-model and file-exchange based CFD/structure coupling). To predict precise temperatures for the whole vehicle, fully-coupled unsteady simulations are required (in the following named: CoNF<sup>2</sup>aS<sup>2</sup> FSI simulation). The CoNF<sup>2</sup>aS<sup>2</sup> FSI simulation is performed along the whole trajectory including the launch phase as well as the re-entry flight phase and considering the material properties through coupling using a high fidelity structural model.

Figure 8(b) illustrates exemplary the result of the CoNF<sup>2</sup>aS<sup>2</sup> FSI simulation during the belly-up flight phase, which is applied to assess stability along the longitudinal roll axis. This results to huge temperature gradients, because the fin at the rear stands in the flow. Beside the fin and canards, another critical element, which requires particular attention during the pre-analyses, is the wrap-up around GPS antenna due to the special material: visible as ring around ReFEx directly behind the canards in figure 8(b). CoNF<sup>2</sup>aS<sup>2</sup> predicts an no-exceeding of the critical temperature of the antenna. Each colder region on the surface of the main body and its wings in figure 8(b), is caused by an underlying structural body, e.g. flanges, ribs under the outer shell, acting as a heat sink reservoir, representing the high quality of the structural model used in this work.

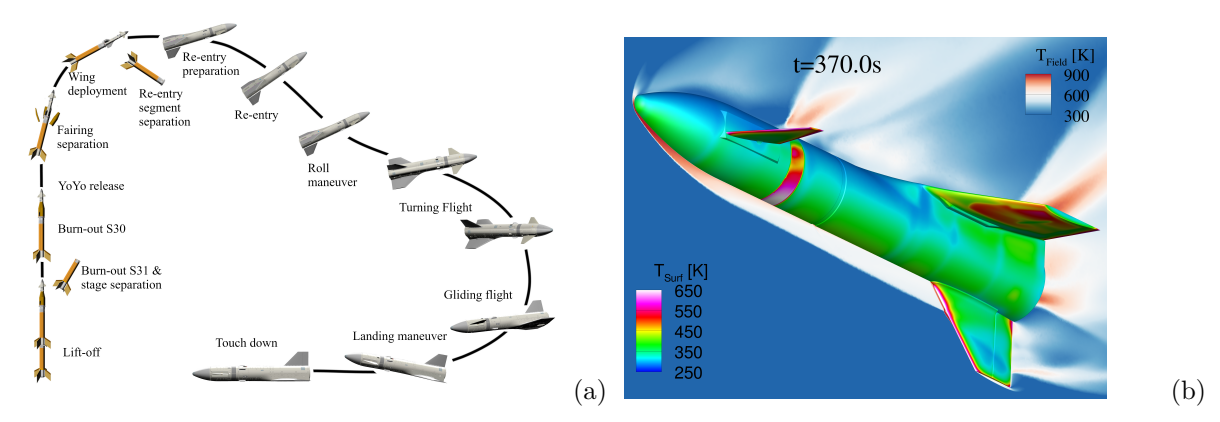


**Fig 8.** Mission overview and key flight maneuver (a) and flow topology during belly-up flight phase at  $t = 370 \,\mathrm{s}$  (b), reprinted from [15].

As expected, the V-model and file-exchange based CFD/structure coupling delivers more conservative results for the temperature distribution in most surface areas. Due to the reduced number of CFD simulations instead of an unsteady fully coupled  $\text{CoNF}^2\text{aS}^2$  simulation, the calculation time can be reduced in general for this chosen approach of structure layout. The time accurate  $\text{CoNF}^2\text{aS}^2$  simulation along the trajectory delivers more precise temperatures. The peak differences of the predicted temperatures on the canards for example are predicted about  $\Delta T = 79\,\text{K}$  to  $\Delta T = 413\,\text{K}$  at the leading / trailing edges higher by the database exchange based CFD/structure coupling but compare well on the surface between. The main body of ReFEx is well captured in both methods differing at worst on the nose cone by 17% at the time point of peak heating at  $t=44\,\text{s}$ . The prediction of the fin varies between 21 K to 121 K, depending on the selected flight phase. Consult Franze et al. [15] for the whole, detailed analysis.

The V-model and file-exchange based CFD/structure coupling delivers intended higher temperatures to be on the safe side during the layout and design phase. To predict precise temperatures for the whole vehicle, time accurate fully coupled unsteady CoNF<sup>2</sup>aS<sup>2</sup> simulations are required and can be used for a final proof of temperature-sensitive components, like the wrap-up around GPS antenna.

One example of the next steps in the upgrading process of CoNF<sup>2</sup>aS<sup>2</sup> is the integration of a flight controller. In the case of the ReFEx vehicle, the flight controller is developed by the DLR Institute of Robotics and Mechatronics and will be integrated as black box in the tool chain of CoNF<sup>2</sup>aS<sup>2</sup> to simulate the whole flight, including the complex roll maneuver of ReFEx.

### 6.2. Panel flutter

Aerothermodynamic loads on high speed vehicles and the structural response of its surface lead to a coupled physical problem. The behavior of this fluid-structure interaction is often non-linear and path-dependent. The observed effects ranges from capacitive cooling to melting of the structure and from steady thermal buckling to limit cycle oscillations or chaotic flutter behavior up to mechanical structural failure.

The  $\text{CoNF}^2\text{aS}^2$  simulation environment has been applied to a thin flexible metallic panel excited by an impinging shock wave in turbulent flow. The simulations are based on tests carried out in the RC-19 facility at the US Air Force Research Laboratory (ARFL) in Dayton/Ohio [6, 7]. The test case set-up is shown in figure 9. The cross section of the RC-19 test section is  $131.1 \times 152.4\,\text{mm}$ . The thin flexible steel panel is mounted flush with the upper wall. The size of the panel is  $253.9 \times 127.0 \times 0.635\,\text{mm}$ . The panel and its outer frame consists of a single part and is manufactured by milling out a solid block. On the lower side of the test section a  $12^\circ$  wedge acts as shock generator. The upstream part of the wind tunnel, including the Mach 2 nozzle, was calculated separately and is not shown here. These simulation provides the inflow data for the test section, which are specified on the inflow plane using a Dirichlet boundary condition. An extrapolation condition is used on the outflow plane. The pressure in the closed cavity

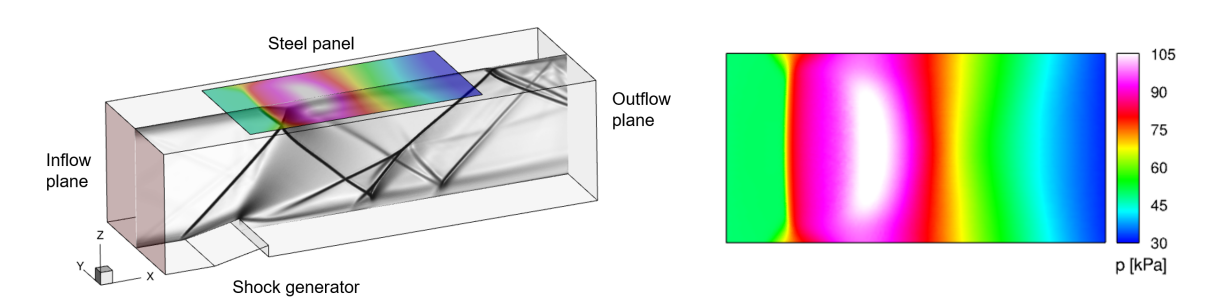
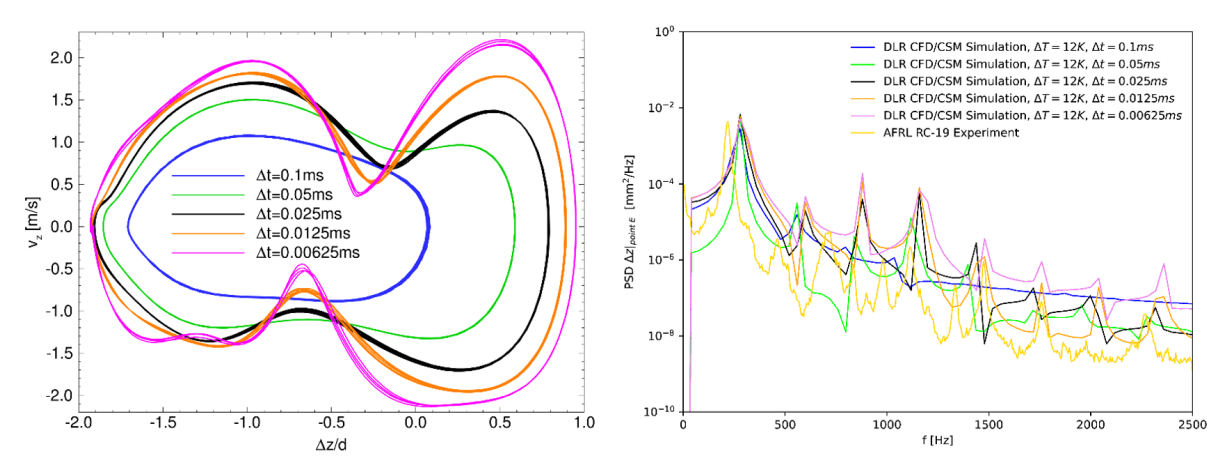


Fig 9. Computational domain of the test section with flexible steel panel and shock generator (a) and panel surface pressure distribution (b).

above the panel is adjustable. All walls are modeled as adiabatic non-slip fully turbulent boundaries. The test gas is assumed to be calorically perfect air. A Reynolds stress model (RSM) turbulence model is used. The Mach number of the free stream in the inflow plane of the test section is around 1.92.

The center plane of the channel in figure 9 shows a simulated shadow graph. The flexible undeformed panel shows the surface pressure distribution. Both results of a stationary calculation, the starting point for the fully coupled FSI simulation. During the wind tunnel run the walls and especially the panel is heated by the flow. Thin structures heat up much faster than thicker ones, so that the frame acts as a heat sink for the panel. This effect leads to a temperature difference  $\Delta T$  between panel and frame and thus to thermal stresses due to thermal expansion. These thermal stresses, together with the pressure difference between the test section and the cavity, cause the panel to buckle. In the simulations the temperature difference effect is modelled in the structure mechanic solver. The temperature of the panel is set to constant homogeneous value of 368 K while the reference temperature (temperature of the frame) is lowered by the difference of  $\Delta T = 12$  K.

After a transient phase a limit cycle oscillation of the panel is observed. Figure 10(a) shows the phase-space trajectory of the panel center point, plotted is the velocity of the center point versus the dimension-less point displacement for different simulated time-steps. Results with larger time-steps serve as starting solutions for calculations with smaller time-steps. The smaller the time-steps the higher the observed frequency components in the oscillation. One reason could be the high resolution of the structural panel mesh of  $2\,\mathrm{mm}$ . The high number of degrees of freedom allows the simulation of small wavelengths and thus high-frequency oscillations.



**Fig 10.** Phase-space trajectory (a) and PSD (b) for the center point of the panel. Plotted are results for different simulated time-steps.

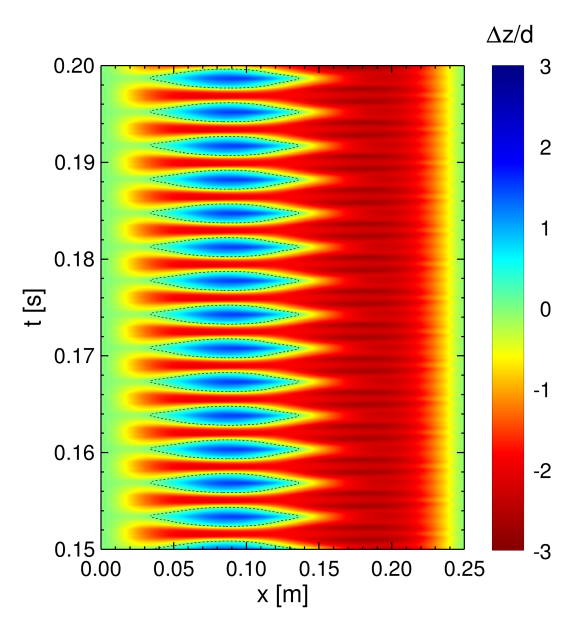


Fig 11. Time-history plot of the simulated panel oscillation with a time-step of 0.0125 ms. The dimensionless displacement  $\Delta z/d$  of the panel center line versus time t is plotted.

The power spectral density (PSD) shows how the power of a signal or a time series is distributed with frequency. The PSD of the center point oscillation is compared with experimental results provided by AFRL in figure 10(b). The results shows again higher-frequency components for smaller simulated time-steps. The oscillation of the complete panel centerline is illustrated in figure 11 for the time-step of 0.0125 ms A detailed description of the panel flutter simulations and the results is given in [30].

### 7. Conclusion

The status overview of CoNF<sup>2</sup>aS<sup>2</sup>, summarized in this paper, is concentrated on the core application of CoNF<sup>2</sup>aS<sup>2</sup>: fluid-structure interaction. The examples shown here highlight the importance of considering multiple challenges associated with hypersonic flight and the herein performed approach: multidisciplinary simulations via the coupling environment CoNF<sup>2</sup>aS<sup>2</sup>.

The examples showcase the wide range of applications for CoNF<sup>2</sup>aS<sup>2</sup>: post-flight analysis (SHEFEX II, chapter 3.1), detailed investigations (rocket nozzle, chapter 3.2), fast reaction on spacecraft-related questions with mid-term approach (chapter 4), layout process with low-fidelity approach (chapter 5) and pre-flight analyses of ReFEx (chapter 3.1). Besides this diversity of applications, the paper highlights the necessity of different accuracy levels. A balance between numerical effort and accuracy is essential, depending on the scientific question and the available time to answer this question. Three fidelity levels are provided in CoNF<sup>2</sup>aS<sup>2</sup>: high-fidelity (simulation time: about months), mid-fidelity (simulation time: about days) and low-fidelity (simulation time: about hours). The paper shows that each approach is important, especially the possibility to switch between accuracy levels. With CoNF<sup>2</sup>aS<sup>2</sup>, a tool environment is implemented, where the motto "high-fidelity if necessary and low-fidelity as possible" can be easily performed.

The results of the analyses demonstrate that the  $\text{CoNF}^2\text{aS}^2$  tool chain is capable of providing realistic simulations of space transportation vehicles. For example, the  $\text{CoNF}^2\text{aS}^2$  validation is demonstrated for the shown flight range of SHEFEX II and its resulting flow phenomena (chapter 3.1). The post-flight analysis demonstrates that the uncertainty of the numerical results is less than in the flight experiment. The only limitations is given by the capabilities of the applied codes. Hence, the development of  $\text{CoNF}^2\text{aS}^2$ 

and its including tools is an ongoing process, where permanently other flow phenomena (e.g. panel flutter, chapter 6.2) and flight ranges are investigated. The upgrades take place through wind tunnel experiments as well as flight experiments. One example for the next steps in the CoNF<sup>2</sup>aS<sup>2</sup> environment is the establishment of rarefied gases to achieve a complete flight range for e.g. another applications, like satellites and their re-entries.

### Acknowledgements

The authors gratefully acknowledges the CFD development team at the German Aerospace Center (DLR), as well as the scientific support and HPC resources provided by DLR. The HPC system CARA is partially funded by the Saxon State Ministry of Economic Affairs, Labour and Transport and the Federal Ministry of Economics and Climate Protection. The HPC system CARO is partially funded by "Ministry of Science and Culture of Lower Saxony" and "Federal Ministry for Economic Affairs and Climate Action".

### References

- [1] Anderson, J. Hypersonic and High-Temperature Gas Dynamics. American Institute of Aeronautics and Astronautics, Inc., Reston, Virginia, 2006.
- [2] Barth, T., Dankert, C., Roden, G., and Martinez Schramm, J. Investigations to the response time of a glued thermocouple on the basis of experimental and numerical analyses. New Results in Numerical and Experimental Fluid Mechanics VII, 2010.
- [3] Barth, T. and Longo, J. Advanced aerothermodynamic analysis of SHEFEX I. Aerospace Science and Technology, 14(8):587–593, December 2010.
- [4] Barz, F. and Franze, M. Comparison of different fidelity approaches for the coupled aerothermodynamic heating of hypersonic reentry vehicle. In HiSST - 3nd International Conference on High-Speed Vehicle Science Technology, 2024.
- [5] Bowcutt, K., Anderson, J., and Capriotti, D. Viscous optimized hypersonic waveriders. 25th AIAA Aerospace Sciences Meeting, 1987.
- [6] Brouwer, K. R., Perez, R. A., Beberniss, T. J., Spottswood, S. M., and Ehrhardt, D. A. Experiments on Thin Panel Excited by Turbulent Flow and Shock/Boundary-Layer Interaction. *AIAA Journal*, 59(7):2737–2751, 2021.
- [7] Brouwer, K. R., Perez, R. A., Beberniss, T. J., Spottswood, S. M., and Ehrhardt, D. A. Evaluation of reduced-order aeroelastic simulations for shock-dominated flows. *Journal of Fluids and Structures*, 108, 2022.
- [8] Cummings, R. Aerothermodynamic challenges of hypersonic flight. AVT-SET-SCI-396 Research Symposium, 2024.
- [9] Eggers, T. and Franze, M. SHEFEX I + II post-flight analysis: Starting point for a virtual flight test environment. In 68th International Astronautical Congress, 2017.
- [10] Franze, M. SHEFEX II a first aerodynamic and atmospheric post-flight analysis. In AIAA Atmospheric FlightMechanics Conference, 2016.
- [11] Franze, M. SHEFEX II an aerodynamic and structural post-flight analysis. In AIAA Atmospheric FlightMechanics Conference, 2016.
- [12] Franze, M. Fluid-structure coupled post-flight analysis of the ascent phase of SHEFEX II. In AIAA SciTech Forum, 2026.
- [13] Franze, M. and Barz, F. Verification of models for aerothermal load prediction using coupled trajectory simulations of a high lift reentry vehicle. In *NATO STO*, 2024.
- [14] Franze, M. and Donn, P. Analysis of weather balloon data to evaluate the aerodynamic influence on the launch phase of SHEFEX II. *CEAS Space Journal*, 15(6):881–894, September 2023.

- [15] Franze, M., Wartemann, V., Merrem, C., Elsäßer, H., Ruhe, T., Eggers, T., and Weihs, H. Aerothermal loads analysis of refex by coupled fluid-structure simulations. CEAS Space Journal, 17(4):513–527, May 2025.
- [16] Génin, C. and Stark, R. and Jack, S. Flow Separation in Out-of-Round Nozzles, a Numerical and Experimental Study. *Progress in Flight Physics*, 7:269–282, 2015.
- [17] Jack, S. and Génin, C. Flow Separation Study in Stiff Ovalized Rocket Nozzles, Part II: Numerical Approach. In 51st AIAA/SAE/ASEE Joint Propulsion Conference, Orlando, USA, 2015. AIAA.
- [18] Jack, S. and Oschwald, M. Simulation of Fluid Structure Interaction in Overexpanded Cold Gas Rocket Nozzles using the DLR TAU Code. In 7th European Conference for Aeronautics and Space Sciences (EUCASS), Mailand, Italy, 2017.
- [19] Jack, S. and Oschwald, M. and Eggers, T. Mechanisms Contributing to the Dynamic Stability of a Flexible Subscale Rocket Nozzle. *Journal of Propulsion and Power*, 40(1):14–24, January 2024.
- [20] Jack, S. and Stark, R. Design and Preliminary Numerical Analysis of a Flexible Structure for a Cold Gas Nozzle Experiment. In 2nd International Conference on Flight Vehicles, Aerothermodynamics and Re-entry Missions and Engineering, Heilbronn, Germany, 2022.
- [21] Kaufman, L. G., II. Pressure estimation techniques for hypersonic flows over blunt bodies. *Journal of Astronautical Sciences*, 1963.
- [22] Langer, S. and Schwöppe, A. and Kroll, N. The DLR Flow Solver TAU Status and Recent Algorithmic Developments. In 52nd Aerospace Sciences Meeting, National Harbor, Maryland, January 2014. American Institute of Aeronautics and Astronautics.
- [23] Laureti, M. and Karl, S. Aerothermal databases and load predictions for retro propulsion-assisted launch vehicles (retalt). CEAS Space Journal, 14(3):501–515, January 2022.
- [24] Lighthill, M. Oscillating airfoils at high mach number. Journal of the Aeronautical Sciences, 1953.
- [25] Mack, A. and Schäfer, R. Fluid structure interaction on a generic body-flap model in hypersonic flow. *Journal of Spacecraft and Rockets*, 42(5):769–779, September 2005.
- [26] Mack, A. and Hannemann, V. Validation of the Unstructured DLR-TAU-Code for Hypersonic Flows. In 32nd AIAA Fluid Dynamics Conference and Exhibit. AIAA Paper 2002-3111, 2002.
- [27] Merrem, C., Wartemann, V., and Eggers, T. Preliminary aerodynamic design of a reusable booster flight experiment. *CEAS Space Journal*, 12(3):429–439, April 2020.
- [28] Merrem, C., Wartemann, V., and Eggers, T. Aerodynamic Data Set Generation for the Experimental Vehicle ReFEx. Springer International Publishing, 2021.
- [29] Morgan, R. Australian hypersonics: Legacy and future directions. STO-MP-AVT-307 PAPER NBR 25, 2018.
- [30] Reimann, B. and Franze, M. and Jack, S. and Barz, F. and Wartemann, V. Coupled Fluid-Structure Simulations of a Clamped Panel at High Speed. In *HiSST 4nd International Conference on High-Speed Vehicle Science Technology*, number 2025-0258, Tours, France, 2025.
- [31] Reimer, L. The FlowSimulator—a software framework for cfd-related multidisciplinary simulations. In European NAFEMS Conference Computational Fluid Dynamics (CFD), 2015.
- [32] Reimer, L. and Heinrich, R. and Geisbauer, S. and Leicht, T. and Görtz, S. and Ritter, M. R. and Krumbein, A. Virtual Aircraft Technology Integration Platform: Ingredients for Multidisciplinary Simulation and Virtual Flight Testing, 2021.
- [33] Rickmers, P., Bauer, W., Kottmeier, S., Delovski, T., Suhr, B., and Klinkner, S. Flight experiment ReFEx: Agile aiv processes for prototype flight experiments. In 73rd International Astronautical Congress (IAC). IAC-22-D2.6.4x68659, 2022.

- [34] Schwamborn, D. and Gerhold, T. and Heinrich, R. The DLR TAU-Code: Recent Applications in Research and Industry. European Conference on Computational Fluid Dynamics. In ECCOMAS CFD, 2006.
- [35] Weihs, H., Longo, J., and Turner, J. The sharp edge flight experiment SHEFEX II, a mission overviewand status. In 15th AIAA International Space Planes and Hypersonic Systems and Technologies Conference, volume AIAA2008-2542, 2008.